

## LA-UR-20-22030

Approved for public release; distribution is unlimited.

Title: Particle size of several plutonium-238 oxide fuel samples from oxalate precipitation processes

Author(s): Mulford, Roberta Nancy  
Parker, Edward Goodfellow (Ned)

Intended for: Report

Issued: 2020-03-03

---

**Disclaimer:**

Los Alamos National Laboratory, an affirmative action/equal opportunity employer, is operated by Triad National Security, LLC for the National Nuclear Security Administration of U.S. Department of Energy under contract 89233218CNA000001. By approving this article, the publisher recognizes that the U.S. Government retains nonexclusive, royalty-free license to publish or reproduce the published form of this contribution, or to allow others to do so, for U.S. Government purposes. Los Alamos National Laboratory requests that the publisher identify this article as work performed under the auspices of the U.S. Department of Energy. Los Alamos National Laboratory strongly supports academic freedom and a researcher's right to publish; as an institution, however, the Laboratory does not endorse the viewpoint of a publication or guarantee its technical correctness.

# Particle size of several plutonium-238 oxide fuel samples from oxalate precipitation processes

R.N. Mulford and E. Parker

## Abstract

Particle size of  $^{238}\text{PuO}_2$  powders is an important factor in determining the structural integrity of fuel pellets hot-pressed from the oxide powder. Understanding the evolution of particle size during aqueous processing is a first step in assuring control of particle size throughout the pellet formation process. Measured particle sizes are reported here, and discussed in terms of measured particle size changes occurring during calcining, observed aggregation of particulate, and particle morphology. Morphology and aggregation are related to surface energy, which governs granule formation and hot pressing behavior. Results are discussed in terms of reported dependence of oxide morphology on process temperatures and reagent concentrations. [1]

## Introduction

Particle sizes of several samples of  $^{238}\text{PuO}_2$  fuel have been measured at various stages in the aqueous processing sequence. Four samples of fuel after aqueous processing and calcining are described. Two of these calcined samples can be compared with samples measured before calcining. Four examples of feed fuel have been examined. Particle size of one blended lot is also reported.

Feed fuel undergoes radioactive decay in storage, resulting in ingrowth of  $^{234}\text{UO}_2$ . The fuel is repurified immediately before hot pressing to remove the uranium, by dissolution and reprecipitation as Pu(III) oxalate,  $\text{Pu}_2(\text{C}_2\text{O}_4)_3$ . The Pu(III) oxalate is used rather than the Pu(IV) oxalate because of the larger particle size of the Pu(III) product, which results in more rapid precipitation and more facile filtration. Although the oxalate decomposes spontaneously to oxide with substantial preservation of particle structure, [2][3] mild calcining ( $650^\circ\text{C}$ ) of the oxalate product is used to produce a uniform product of reliable stoichiometry. Blended lots are composed of fuel after calcining, to manipulate the net concentration of impurities in the lot, or to adjust isotopic ratios, if necessary.

The morphology of the pellet is carefully controlled to provide not only strength, but a relatively low density and interconnected porosity which allows escape of helium arising from radioactive decay of the plutonium. [4] Minimization of pellet cracking is important, to allow facile welding and encapsulation of the radioactive material, and to ensure that no particulate is generated from the pellet during handling. A minimally fractured pellet is a necessary requirement for safety, as the plutonium oxide remains localized and bound into a solid body.

Measurement of a number of samples from separate batches of fuel subjected to aqueous processing, along with recording of details of execution of each individual batch, might allow control of critical particle size parameters and optimization of the particulate

surface energy and other characteristics. Controlling these parameters might facilitate the most effective hot pressing of the material. In the years since the development of the fuel preparation and hot pressing protocols, the source of the feed fuel has changed and a new source will soon be entering the feed fuel stream. Changing feed fuel may or may not require active optimization of the aqueous processing parameters, but availability of data is necessary to confirm that no radical changes result from such unavoidable process variations. Smith et. al. [1] measured the dependence of precipitate morphology on precipitation temperature, reactant concentrations, and details of the addition of reactants, to provide a roadmap of precipitation behaviors which allows comparison of observed particle sizes to an existing catalog of trends.

Between aqueous processing and hot pressing, fuel is ball-milled to reduce particle size, and then “slugged and screened,” or pressed into granules of a selected size. Further calcining of granules should in principle erase any signature arising from aqueous processing. However, particle morphology arising during aqueous processing appears to affect subsequent behavior of the fuel, [5] and particle size is strongly related to morphology in oxalate precipitates. [2][6] Effective filtering of the precipitate from the aqueous process also depends on particle size and morphology.

Process performance of the oxide powder might be related in a persistent and enduring way to the morphology arising from the aqueous process. If the oxide crystallites are too solid and dense, the surface energy will be low, and will remain low throughout ball milling. The fuel particles may not adhere during slugging, or the formed granules may fracture excessively on screening. Efforts to press feed fuel or to delete processing steps have been made, and are observed to result in a completely incoherent pellet. [2][5]

Age of the fuel is likely to be another relevant factor, since helium ingrowth is known to fracture fuel particles. [7] Apparent disintegration of granulated fuel into fine powder has been observed during processing delays. [9] Retention of low-fired material for even 48 hours results in poor cohesion during hot pressing. [5] Behavior in hot-pressing suggests that the surface energy is reduced over time, possibly as asperities are removed by annealing during storage. Particle size has been reported to change with time. [6]

Safety basis calculations and the establishment of Material at Risk (MAR) limits governing inventories allowing  $^{238}\text{Pu}$  operations are also dependent on particle sizes, and require data regarding the particle sizes that may be present in any given location at any stage during aqueous processing. Smaller particles are more mobile and more easily distributed during a catastrophic failure of building containment features, and thus batch quantities may be constrained according to particle size. Studies of size distribution produced by ball-milling  $^{238}\text{PuO}_2$  oxide have been performed to assist with MAR determination for the process. [10]

The particle sizes of four post-aqueous (PT lots) lots are reported, two of them before and after calcining. Particle size of one blended (AQR) lot and particle sizes of some feed fuel lots are also presented. Variation within the small ensemble of different aqueous runs is examined. Changes occurring between auto calcining and subsequent high-temperature calcining are described. This summary includes measurements made in 2012 of aqueous fuel lot PT 236R and feed lot SN 175.

## Particle Size Measurement by Direct Optical Imaging

Particle size can be measured by several methods. Microscopic imaging of particles suspended in ethylene glycol was used to obtain the data reported here. Microscopic examination of particles is well-suited to analysis of material with a large range of sizes, and to particle size distributions which are not monomodal such as those arising from chemical processing and precipitation. Agglomeration of particles is known to occur in  $^{238}\text{PuO}_2$  precipitates, [2][6] making direct imaging one of the few reliable methods of accurately evaluating the sizes of particles and determining the extent of agglomeration. The limitation of the optical imaging method used here is in resolving particles smaller than 1  $\mu\text{m}$ . The NIH freeware *Image J* is used to analyze images. [11]

Historically, particle sizes in  $^{238}\text{PuO}_2$  operations have been monitored using laser diffraction. In particular, particulate arising from ball-milling step of the fuel processing sequence was measured. Laser diffraction is suitable for measuring a narrow range of particle sizes, and is applicable to sizes below 10  $\mu\text{m}$ . The results obtained for ball-milled material using microscopic analysis differ from the historical measurements. [10] Disagreement between direct microscopic observation and other particle size measurement methods is a well-known phenomenon. [12] Comparison of data sets is best done within measurements obtained by similar methods.

Samples from the various processing steps are received in glass vials containing a few milligrams of oxide each. The particulate is suspended in a few milliliters of ethylene glycol, which is sufficiently viscous to keep the particulate in suspension during sample preparation. It is not known whether any fraction of the sample adheres to the glass, but no visible residue remains in the vial. A drop is placed on a microscope slide, and the particles settle into the focal plane. One slide yields a number of images. During settling, independent particles can overlap, obscuring the size of particles. This problem can be remediated to a degree during analysis, both manually and via algorithms available in the software.

After separation of obviously overlapping particles, Image J analysis of the particle image yields histograms of the particle sizes, including images that may be either agglomerates or extended particle morphologies. Because agglomerates may obscure the dimension of individual particles, a second analysis is performed on each image. In order to determine the size of individual particles, all potentially overlapping or agglomerated particles are erased from the image, removing all but isolated particles. Image J analysis of remaining (isolated) particles provides a characterization of small single particles in the mixture.

It is possible that agglomerates represent the effective particle size, but individual particles probably best represent the characteristic size and morphology arising from the aqueous process conditions, as described by Smith et. al. [1] Culling of the image to remove agglomerates is done by hand in a labor-intensive process, in order to evaluate only non-agglomerated particles. A certain amount of judgement enters into image preparation, separation of particles that touch, and decisions as to what particles are joined and which pairs are simply overlapping individual particles. Comparison of the

analysis of individual images by different analysts indicates that slight variations in populations of individual sizes has some influence on the overall profile, particularly for larger particle sizes, which may be judged to be overlapping and removed.

Sample preparation can affect the number of overlapping particles if the density of particles is large on the slide. Small particles are less likely to overlap than large ones, so a dense image tends to select slightly for small particles, once the overlapping complexes of particles are eliminated from consideration.

Particle size histograms are expressed in terms of particle volume, although the measured quantity is particle area in the images. Transformation of 2-D particle images to particle volume assumes spherical particles, an assumption that is more appropriate for some images than for others. In general, the PuO<sub>2</sub> particles tend not to be strongly anisotropic, although particles with random, lobed morphologies have been described in the past [3] and are likely encountered in the fuel described here. Particles comprising feed fuel are flat square particles, for which a spherical approximation is not ideal, but does allow comparison with other populations. Presentation of particle size data as a percentage of volume emphasizes large particles over smaller ones.

Differential plots are generated by plotting the population in 1- $\mu$ m increments. Cumulative plots describe that fraction of particles less than or equal to a given size. Superposition of differential and cumulative plots provides an illuminating picture of the distribution of particle sizes. Smoothing the data by averaging over 10- $\mu$ m intervals provides a more comprehensible picture of the distribution by suppressing variability between 1- $\mu$ m bins.

## Results

Particle size measurements for aqueous process samples are presented below. Analyzed samples were obtained from aqueous lots PT 275R, PT 276R, and PT 279R, supplementing analyses of PT 236R done previously. Blended lot AQR 202 was also measured. Analyses of particle images by two separate analysts provides reassurance that the judgement used to distinguish overlapping particles from agglomerates or complex shapes is not perturbing the overall measurement of populations at various sizes. For example, analysis of PT 275 by two separate analysts are compared in Figure 1. Both histograms of particulate from post-aqueous lot PT 275R are similar, with maxima at 140  $\mu$ m and 170  $\mu$ m to 180  $\mu$ m and a population extending to 260  $\mu$ m.

Analysis of those particles from lot PT 275R which are unambiguously single particles yields the histogram shown in Figure 2. These particles comprise about 10% of the total number of particles measured. The image shows a broad maximum in particle size at approximately 40  $\mu$ m and a secondary maximum at 48  $\mu$ m.

Particles from lot PT 276R are shown in Figure 3. The distribution shows a broad distribution with maxima at 80  $\mu$ m and 100  $\mu$ m and a large population of particles between 150  $\mu$ m and 230  $\mu$ m. A substantial number of particles smaller than 50  $\mu$ m is evident.

Particulate from lot PT 279R is shown in Figure 4, along with a culled image in which analysis is restricted to single particles from lot PT 279R. The broad particle distribution in PT 279R shows maxima at 85  $\mu\text{m}$  and 120  $\mu\text{m}$ , and a uniform distribution of larger particles. Single particles range in size from 15  $\mu\text{m}$  to 45  $\mu\text{m}$ , with a maximum at approximately 36  $\mu\text{m}$ .

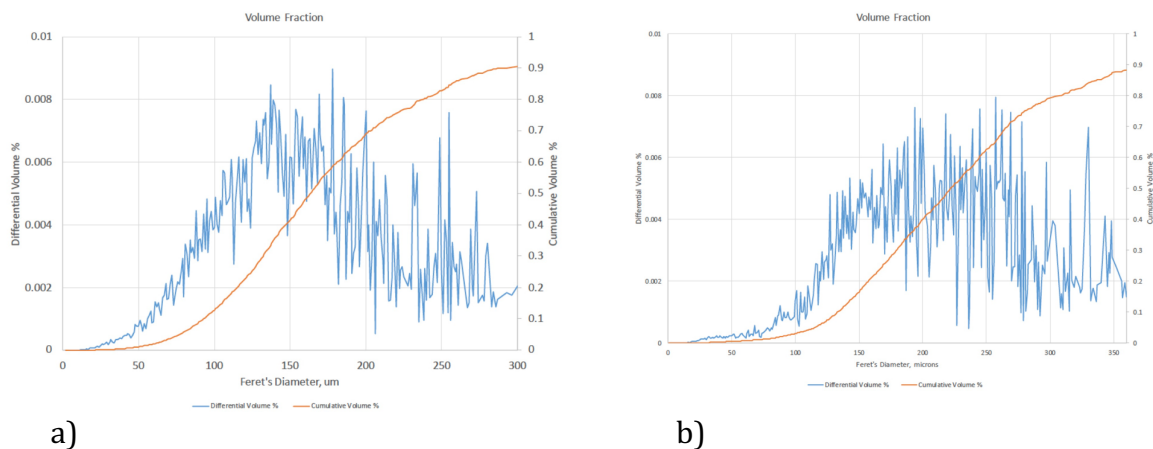


Figure 1. PT 275R a) analysis by Kayla Gill b) analysis by Ned Parker

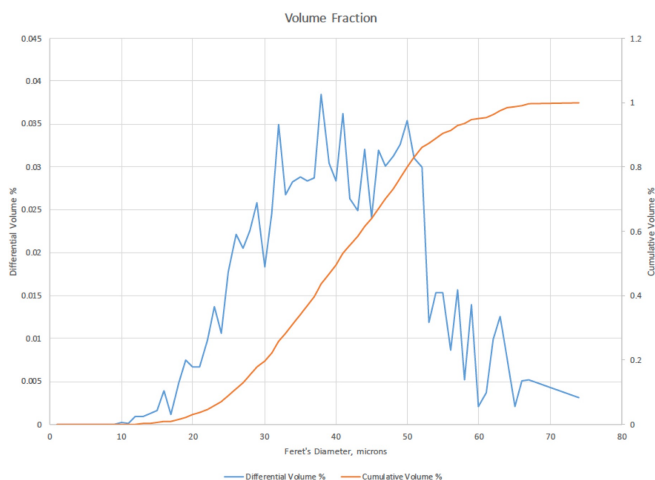


Figure 2. PT 275R (Ned) showing only individual particles.

Analysis of an older aqueous lot, PT 236R, measured in 2011, is added for comparison, as Figure 5. A maximum particle size of 47  $\mu\text{m}$  is seen, with no larger particulate or agglomerates.

The blended lot AQR 202 is composed of multiple PT lots, and should reflect the particle size distributions of typical PT lots, unless the sample was acquired after ball-milling and slugging/screening. Data for blended lot AQR 202 is shown in Figure 6. This AQR lot

exhibits a maximum particle size smaller than 20  $\mu\text{m}$ , and few particles larger than 80  $\mu\text{m}$ , particle sizes consistent with a sample acquired after ball-milling

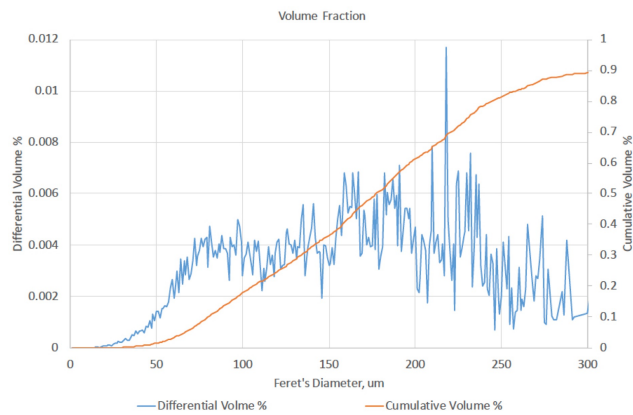
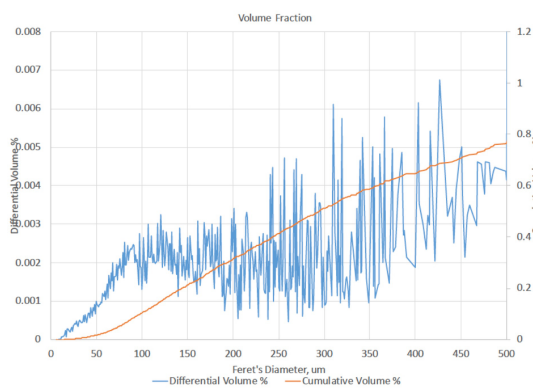
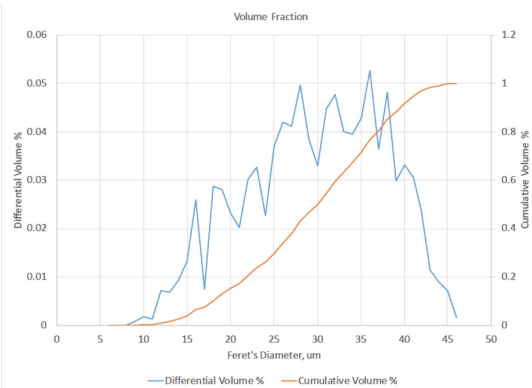


Figure 3. PT 276R (Kayla)



a)



b)

Figure 4. PT 279R, a) all particles and b) with analysis restricted to individual particles.

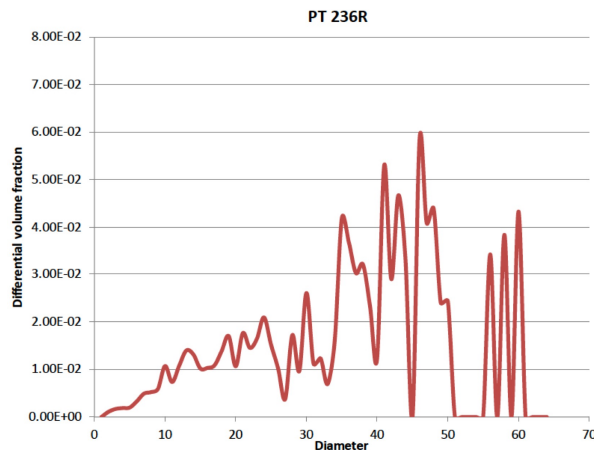


Figure 5. PT 236 R smoothed data

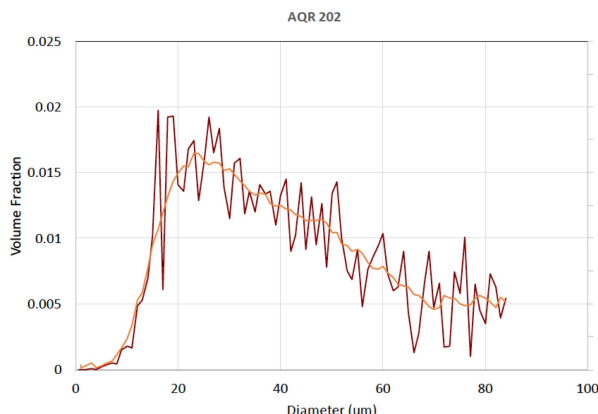


Figure 6. Blended lot AQR 202, detailed and smoothed data

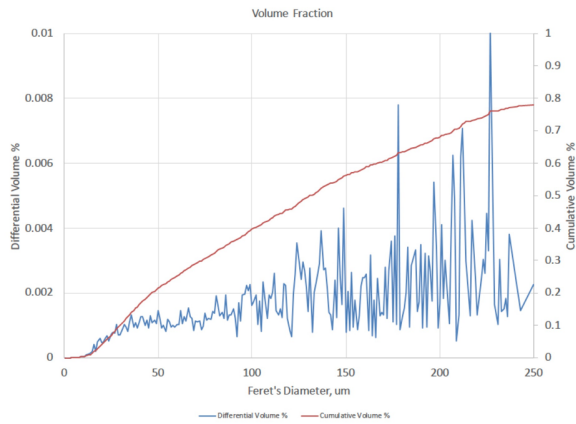
### Changes on Calcination: Auto-calcined and Furnace-calcined particles

After precipitation of the  $^{238}\text{Pu}$  oxalate, the oxalate cake is dried and allowed to spontaneously decompose in air to oxide. The heat of decomposition and the high temperature maintained by the  $^{238}\text{Pu}$   $\alpha$ -decay promote auto-calcination of the oxide product. The auto-calcined material is then heated in a furnace at  $650^\circ\text{C}$  for 2 hours to provide uniform calcination conditions for all material. Samples taken before (“pre-calcined”) and after the deliberate calcining step are compared.

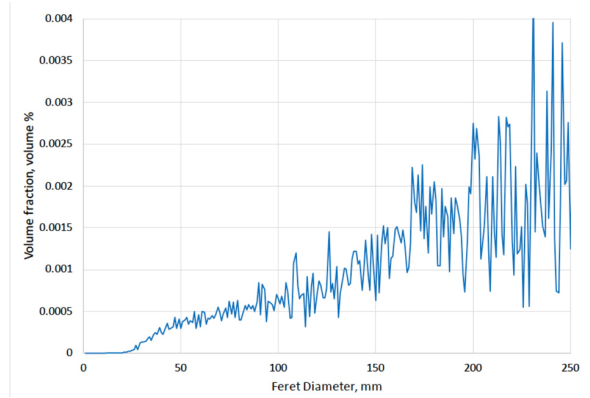
Samples obtained before calcining exhibited a distinctly yellow color suggesting that either some oxalate or carbon [6] was present in the sample. In general,  $^{238}\text{Pu}$  oxalate is hot enough to be expected to spontaneously decompose completely to the oxide, and pre-calcined samples are assumed to be composed entirely of oxide formed at a somewhat lower temperature than the batch calcining temperature.

Pre-calcined oxide from lot PT 275R that was sampled after auto-calcining but before deliberate calcining is shown in Figure 7. Both analyses show a fairly uniform distribution from  $50\text{ }\mu\text{m}$  to  $150\text{ }\mu\text{m}$ . Figure 7a shows a slight maximum at  $28\text{ }\mu\text{m}$ . Figure 7b shows many more particles between  $100\text{ }\mu\text{m}$  and  $260\text{ }\mu\text{m}$ , with a slight maximum around  $60\text{ }\mu\text{m}$ . The differences between the two analyses indicate the extensive population of agglomerated particles, and the differences in judgement as to where to divide overlapping particles.

Oxide from auto-calcination of lot PT 276R is shown in Figure 8. This pre-calcined material exhibits a distinct population of particles in the  $60\text{ }\mu\text{m}$  to  $75\text{ }\mu\text{m}$  range, and a substantial population at  $100\text{ }\mu\text{m}$ . A few particles of large volume dominate the region above  $150\text{ }\mu\text{m}$ .



a)



b)

Figure 7. PT 275R before calcining a) analysis by Kayla and b) analysis by Ned

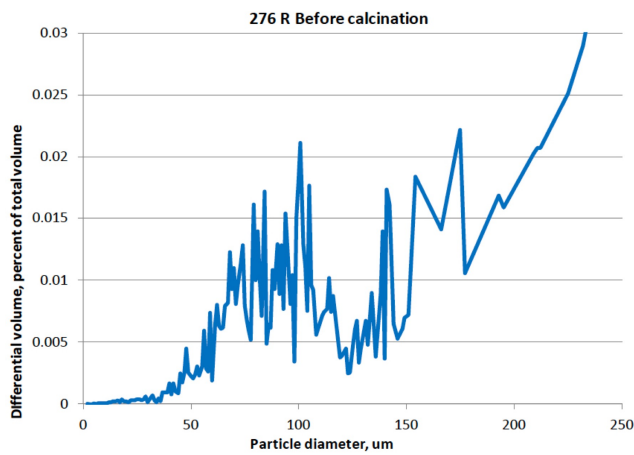
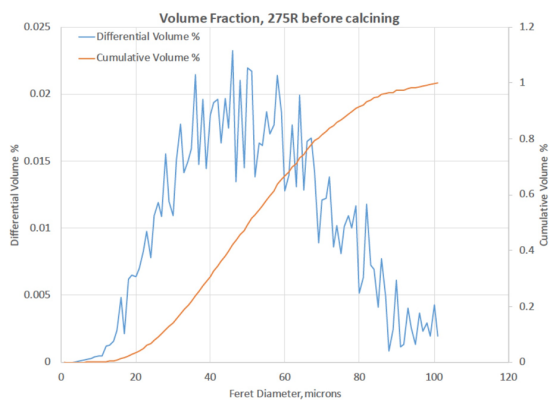
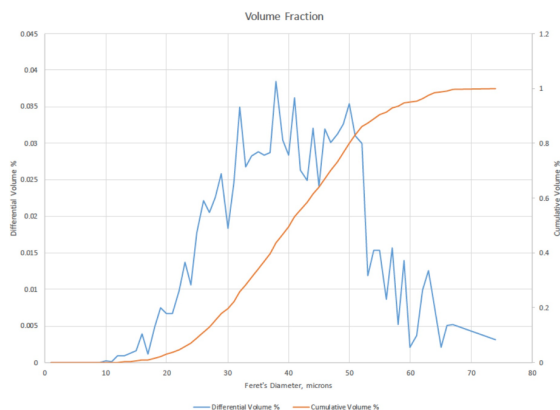


Figure 8. PT 276 R before calcining (Kayla)

Omitting the agglomerated particles from the analysis yields unique information regarding each sample. Examination of individual particles from PT 275R before and after high-temperature calcination shows that the overall shapes of particle size distributions of the individual well-defined particles are similar before and after calcination. Distributions are shown in Figure 9. Calcining of lot PT 275R changes the maximum in the population of individual particles from 48  $\mu\text{m}$  to 38  $\mu\text{m}$ , although the difference between the profiles is minor.



a)



b)

Figure 9. PT 275R individual particles only a) before calcining b) after calcining

Including agglomerates in the analysis provides a complete picture of the product obtained from aqueous processing. Measurements of all particles in lot PT 275R before and after calcining are shown in Figure 10. The population of particles around 35  $\mu\text{m}$  to 50  $\mu\text{m}$  is decreased by calcination, and the population between 125  $\mu\text{m}$  and 140  $\mu\text{m}$  increases, forming a distinct maximum at 140  $\mu\text{m}$ . There are distinctly fewer individual large particles after calcining, with the population of particles between 55  $\mu\text{m}$  and 100  $\mu\text{m}$  dropping noticeably on calcining. Only very small changes are observed in the sizes of the non-agglomerated particles in this lot.

The comparable change in lot PT 276R before and after calcining is shown in Figure 11. Distributions are very similar before and after calcining, exhibiting maxima around 75  $\mu\text{m}$  and 100  $\mu\text{m}$ . While a population of larger particles is present after calcining, the agglomerates above 225  $\mu\text{m}$  appear comprise a smaller relative fraction of the population.

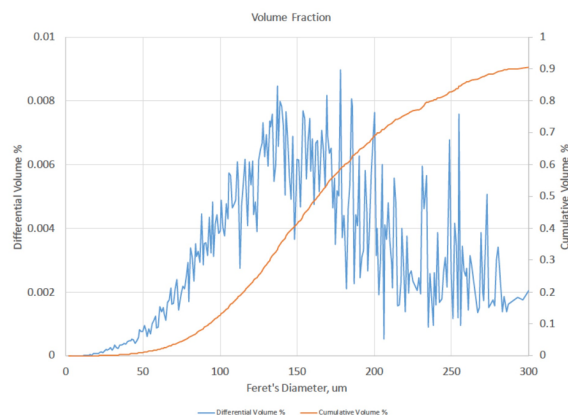
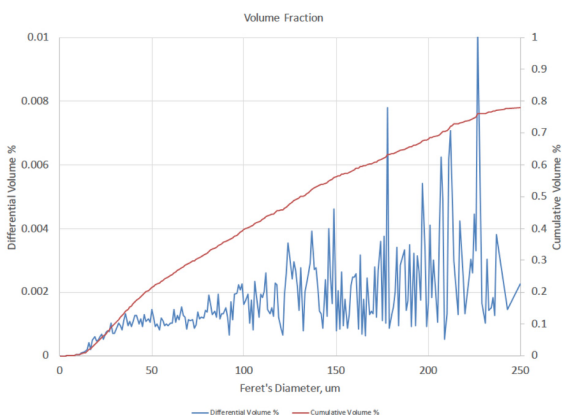
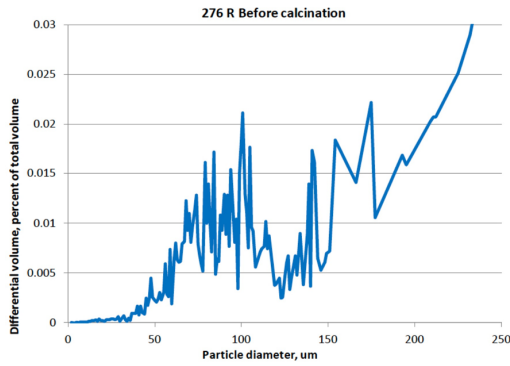
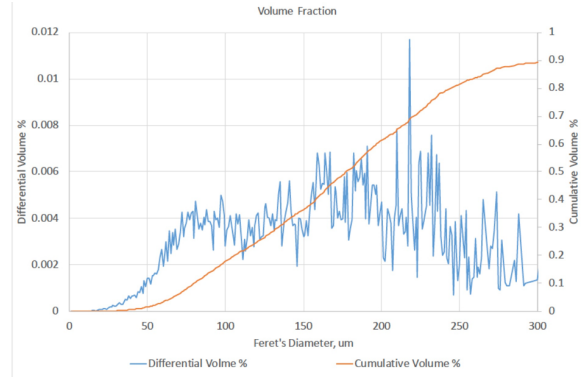


Figure 10. PT 275R, all particles, before and after calcining (Kayla)



a)



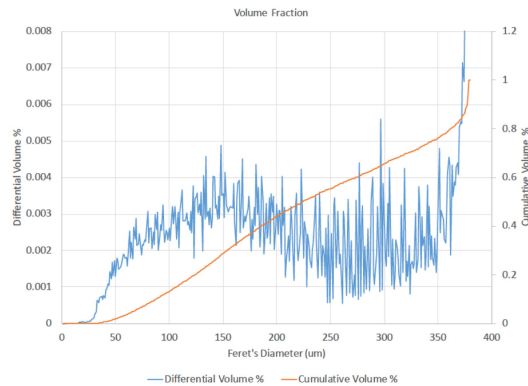
b)

Figure 11. PT 276R a) before calcination and b) after calcination

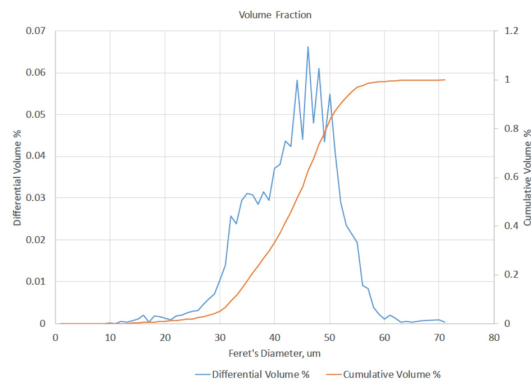
In both PT 275R and PT 276R, the importance of agglomerates larger than 150  $\mu\text{m}$  appears to decrease after calcining. Available data are not sufficient to characterize run-to-run variation, or to compare runs conducted with anomalous rates or temperatures. However, these plots suggest the general sizes and behaviors that appear in particulate from feed fuel and from aqueous processing, and allow comparison with previous measurements. [1]

## Feed Fuel

Particle sizes have been measured for two lots of feed material. Particle sizes for lot FSO-066 are shown in Figure 12. Particle sizes for SN-175 are shown in Figure 13. With inclusion of agglomerated material, feed FSO-66 appears to have a maximum particle size about 150  $\mu\text{m}$ . Individual particles for the two lots are quite different. Lot SN-175 has a distinct maximum between 9  $\mu\text{m}$  and 12  $\mu\text{m}$ , and FSO-66 has a multimodal distribution with maxima between approximately 35  $\mu\text{m}$  and 46  $\mu\text{m}$  and few particles with sizes between 10  $\mu\text{m}$  and 20  $\mu\text{m}$ .



a)



b)

Figure 12. Feed lot FSO-66

a) all particles

b) analysis restricted to individual particles

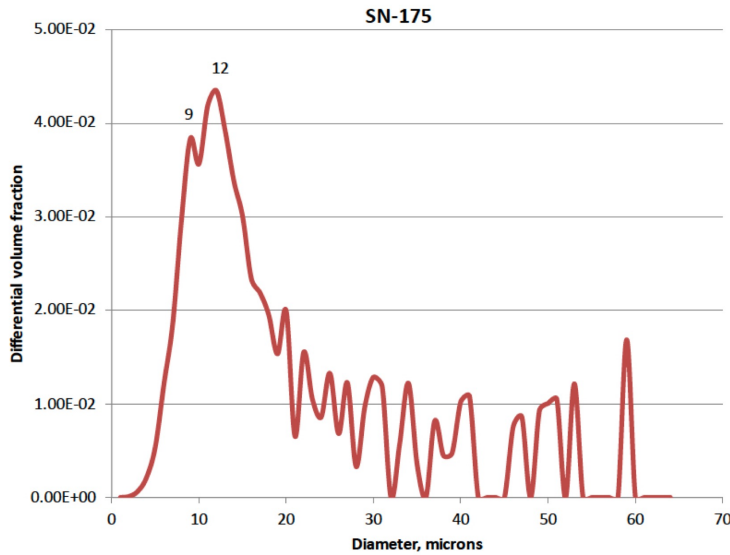


Figure 13. Feed lot SN-175, all particles

The distinction between individual particles and agglomerates is evident in the feed fuel, which exhibits the flat square crystallites typical of material precipitated from Pu(IV) oxalate solution. [3] Images of feed fuel from feed lot FSO-066 are shown in Figure 14. If individual particles are examined, particle size distributions are narrow, but the variation in particle size is large, 12  $\mu\text{m}$  for SN-175 (Figure 13) and about 46  $\mu\text{m}$  for FSO-066 (Figure 12).

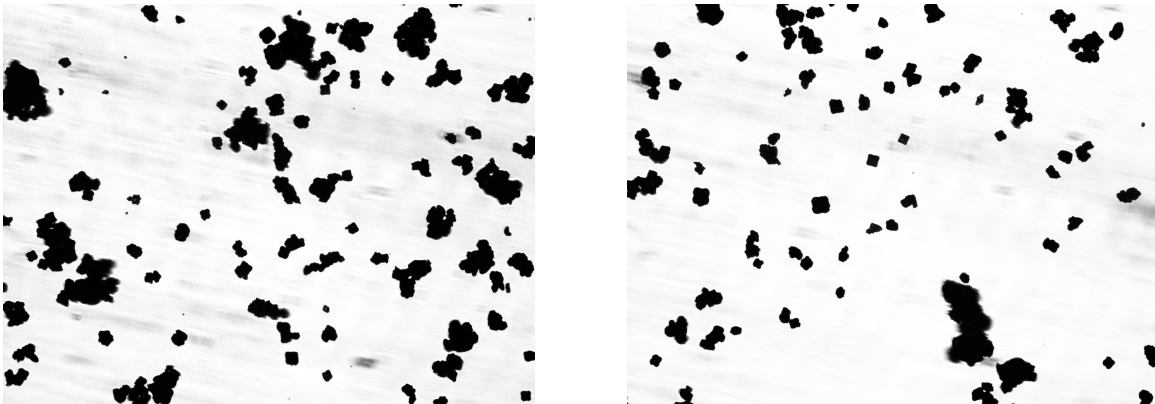


Figure 14. Two images of feed fuel FSO-066, showing typical individual square crystallites and also agglomerates

Where agglomerates are included, feed fuel particle sizes are comparable to particle sizes after aqueous processing. Figure 12a, feed fuel, compares well with Figures 10b or 11b, fuel after aqueous processing and calcining.

## Culled Images to Evaluate Small Particles

The images used for these studies are fairly dense with particles. Diluting the particulate density with ethylene glycol might reduce the apparent agglomerations. However, some degree of agglomeration is likely actual physical adhesion. [3] Other particle size measurement techniques describe these as adherent clumps as “large particles,” obscuring critical information regarding the true character of the material. [1] Adherent clumps are consistent with roughness and with shapes observed by other workers. [3]

Expressing the volume of each particle size as a volume percent of the total volume obscures the fact that the individual particles comprise a small fraction of the total volume of particles. Individual particles and the entire population of particles are compared in Figure 15.

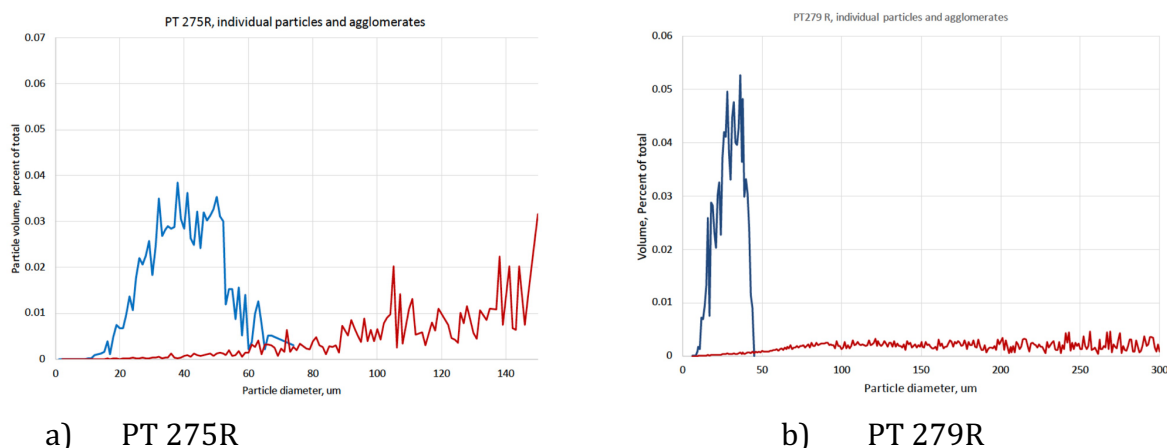


Figure 15. Individual particles and agglomerated particles

Removal of the agglomerates in the images results in similar particle size distributions falling between 30  $\mu\text{m}$  and 50  $\mu\text{m}$  for all samples analyzed. The possibility exists that either selection by the analyst or else the resolution limits of the microscope might be governing the culled distributions. Comparison of culled single-particle distributions for the several samples indicates that differences between sizes of small particles are detected, although distributions are similar. Distributions of single particles from four different sources are compared in Figure 16.

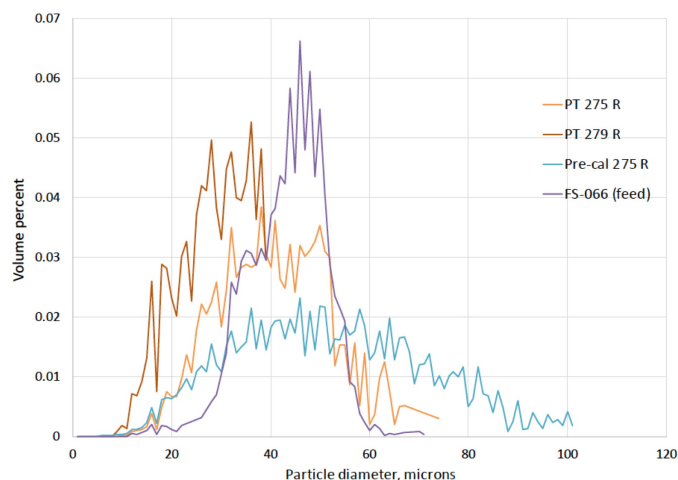


Figure 16. Four culled single-particle images, showing differences between distributions.

## Discussion

Particle size matters because large particles facilitate filtering, and because particle size and morphology can affect all subsequent processing. [5][9] Ball-milling of the precipitate is performed to minimize and normalize the effects of precipitation, but Smith reports that the ball-milling of laths does not produce spherical particles, suggesting that precipitate morphology may not be entirely erased by ball-milling. [1] Rosettes break up to laths in ball milling, suggesting that the degree of rosette formation matters only for the precipitation phase.

The records presented here show large particle sizes and extensive agglomeration, relative to expectations and previous records. Images acquired in 2012 exhibit fewer large particles, for instance lots PT 236R (Figure 5) and AQR 202 (Figure 6). The apparent population of large particles in lots PT 275R and PT 276R may reflect details of the measurement method, specifically the dense particle distributions in the images. Alternately, the large particles and agglomerates may reflect variation between the product of aqueous separations done in 2012, which were executed by a small dedicated staff with long experience of the process, and current operations, in which a large variety of workers participate in runs. The similarity between the single-particle measurements summarized in Figure 16 and measurement of particulate in the 2012 lot PT 236R indicates that the fundamental particle size is similar, and that the presence of agglomerates or overlapping particles is greater in the recent measurements.

Previous workers [1][2][3] could not easily distinguish between single laths, fused rosettes or clusters of lathes, and loose agglomerates, and hence identified all particles larger than the smallest particles as agglomerates. Where SEM imaging could be done, particle morphologies were definitively identified. [3] With care to avoid semantic confusion, previous observations [1][2][3] provide a guide to interpreting data presented here.

The direct imaging used here makes it clear which particles are agglomerates and which are single particles, although overlapping particles are less easily distinguished from agglomerates. Oxalate precipitate consists of laths which can form singly, form loose agglomerates, or fuse into large complex particles or rosettes. Examples are shown in Figure 17. [2] Culling can produce a reliable measure of the dimension of single particles when optical imaging is used for measurement.

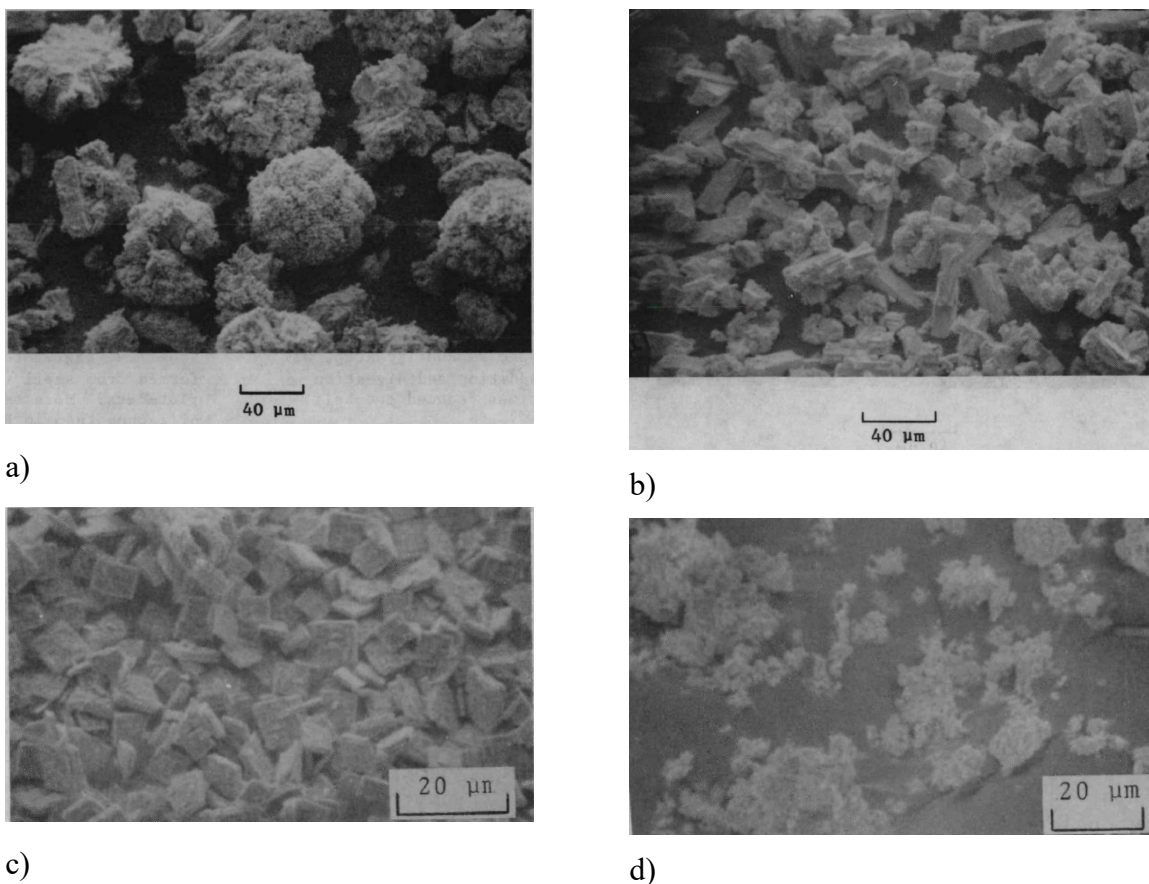


Figure 17. Images of  $\text{PuO}_2$  morphologies from Burney and Congdon [2]

- a) Rosettes from Pu(III) oxalate
- b) Laths and agglomerates from Pu(III) oxalate
- c) Square precipitate from Pu(IV) oxalate
- d) Agglomerates from Pu(IV) oxalate

Observed single particle sizes reported here compare well with previous observations. Historical observations suggest that particles with diameters between  $7\ \mu\text{m}$  and  $60\ \mu\text{m}$  arise from Pu(III) direct strike precipitation. [1] This measure compares well with the  $12\ \mu\text{m}$  to  $55\ \mu\text{m}$  particulate shown in Figure 16. Burney and Smith also report a mode size of  $5\ \mu\text{m}$ , particle sizes up to  $140\ \mu\text{m}$ , and extensive agglomeration up to  $400\ \mu\text{m}$ . [2] However, they used exclusively “reverse strike” production of particulate, adding the Pu(III) solution to the oxalate. [2] Smith reports that rosettes arise from direct strike and laths from reverse strike, so the smaller  $5\ \mu\text{m}$  particles reported in the reverse strike precipitation may reflect a higher population of single laths. [1] Burney and Congdon, using direct strike, observed well-formed rosettes with diameters between  $50\ \mu\text{m}$  and  $100\ \mu\text{m}$ . [3] These observations are consistent with particle sizes reported here. The method used to generate particulate described here is direct strike, with gradual addition

of oxalate to the Pu(III) solution over 20 minutes, to maintain a low and constant oxalate concentration.

Previous workers measured mass as a function of particle diameter, allowing their data to be compared with measurements here, which are expressed as the volume fraction as a function of particle diameter. The density of these types of particles is known to be less than half of the theoretical value, implying that particles are quite porous. [13] Images also suggest high porosity. [3] Variations in the density of agglomerates could result in a slight mismatch between measurements expressed as weight and measurements expressed in terms of volume fraction.

Solubility of the precipitate governs the growth rate of individual particles, while supersaturation of the solution governs the nucleation of new particles. [2] Thus, gradual addition of oxalate and maintenance of the oxalate concentration can be expected to maximize the size of laths and clusters in the samples described here. Reproducible size and particle morphology are historically generally observed in both reverse strike [2] and direct strike [3] processes, because particle size is governed solely by the final solubility of the Pu oxalate and any factors affecting that solubility, including temperature and the concentrations of nitric acid, Pu, and oxalate, rather than by mechanical factors or batch scale.

Smith and Burney [1] give lath size as a function of temperature and concentrations, reporting that lath size increases with temperature from 21°C to 71°C, and increases with decreasing concentration of oxalic acid. They report lath sizes up to 30  $\mu\text{m}$ . [1] Agglomerates show inverse dependence on the same factors because at smaller particle sizes the particle collision rate increases, leading to agglomeration. [14] Thus the gradual addition of oxalate, which produced the particles described here, should minimize oxalic acid concentration and thus maximize lath sizes, to optimize filterability. Burney and Smith observed that the lowest oxalate concentrations led to a 4.5  $\mu\text{m}$  lath size in their reverse strike process. [2]

Temperature matters for formation of Pu(III) oxalate particles discussed here. At higher temperatures, solubility of the precipitate is higher, and lath sizes are larger. [2] Accordingly, higher temperatures should lead to less agglomeration. Temperature is not explicitly controlled for the precipitations examined here. Temperature is near 100°C during dissolution of the impure PuO<sub>2</sub> feed, but falls to a measured temperature of 32°C to 34°C before addition of oxalate. [15] A high degree of agglomeration has been observed at low temperature. At 21°C, 60 weight % agglomeration has been reported, while at 71°C, only 3 weight% agglomeration is observed. [2] The high degree of agglomeration reported here is consistent with expectations for agglomeration at low temperatures. The measured lath sizes of up to 35  $\mu\text{m}$  are large, as anticipated at higher temperatures.

Smith & Burney observe that larger particle sizes and also rosettes are obtained at higher nitric acid concentrations. [1] Rosette formation is pronounced above nitric acid concentrations of 5 M. The process generating the particulate described here requires dilution of nitric acid down to 2 M prior to the reduction step which adjusts the oxidation state of the plutonium. Oxidation state is controlled with hydroxyl amine nitrate (HAN) which is unstable at nitric acid concentrations above 2 M. Burney and Smith observed

for their reverse strike process that, between nitric acid concentrations of 0.5 and 2.5 M, agglomeration was minimized, and that particle size was maximized between 2 and 2.5 M nitric acid. [2] Nitric acid concentrations generating the particles described here should lead to large particles but to very little agglomeration. While large particles are observed, agglomeration appears to be extensive.

Higher plutonium concentration in feed leads to lower particle size in reverse strike. [2] Plutonium concentration is fixed in the direct strike process described here.

Based on these various historical reports, particle sizes reported here are reasonable. Low oxalate concentrations lead to large particles, and a 2.0 M nitric acid concentration leads to large laths but no rosettes. Temperature for formation of the particles presented here has been measured to be 32°C to 34°C, [15] suggesting that small laths and a high degree of agglomeration should be observed. However, For the process described here, the plutonium concentration is relatively high, and should also lead to high agglomeration and small particle size. Relatively large laths are observed, as well as extensive agglomeration.

Since the process temperature is reasonably constant from batch to batch, the single-particle data measured in the culled images is expected to be fairly constant, as observed. (Figure 16.)

Previous work [1][2] was strongly focused on lath dimensions. Because a Coulter counter was used for particle size measurements, previous workers could not distinguish laths from fused agglomerates except by SEM imaging. These workers identified all large particles as agglomerates, and confirmed this identification when the large particles could be broken up by ultrasonic exposure. Burney and Smith cite a mode (lath) size of 0.4  $\mu\text{m}$  and identify anything larger as agglomerates. [2] Compared to 0.4  $\mu\text{m}$ , the lath sizes of 8  $\mu\text{m}$  to 35  $\mu\text{m}$  measured here are very large. Laths can be distinguished from multi-lath composites or agglomerates more easily using direct imaging, and observed sizes can be associated with laths by culling images to measure single particles.

## Calcination

Calcination of the precipitate should largely preserve relevant particle sizes and morphologies. Particle size is determined by precipitation, and not by calcination. [6] Very little contraction of particle sizes is expected on calcination. [2][6] The oxalate ligand decomposes to CO and CO<sub>2</sub> and escapes from the structure as gas, leaving the net particle structure largely intact. [1][2] Burney and Smith report that calcining at 735°C for two hours produces no “sintering,” although micrographs suggest some consolidation within individual particles. [3] Details of the decomposition govern surface area, carbon content, and residual adsorbed species, and both thermal and radiation-induced decomposition are reported to produce similar particles. [6] In particular, surface energy changes on calcining. [1] The mechanism of decomposition can be complicated, with the Pu(III) precipitate undergoing endothermic dehydration and then stepwise decomposition via oxycarbonate (-OCO<sub>2</sub>.) [6] In the case of <sup>239</sup>Pu, Pu(III) can be re-oxidized to Pu(IV) unless blanketed by CO or CO<sub>2</sub>, because decomposition can occur at low temperatures, on the order of 250°C to 350°C. [6] Because <sup>238</sup>Pu oxide auto-calcines at higher temperatures because of the self-heating of the <sup>238</sup>Pu oxide, maintenance of the Pu(III)

oxidation state and the associated particle morphology is probably assured, even in an air atmosphere.

Mandard and Medic see strong dependence of particle size on calcination temperature for  $^{239}\text{PuO}_2$  produced from Pu(IV) oxalate. [16] However, in the range between 450°C and 750°C they report a constant spherical equivalent radius of 3  $\mu\text{m}$  to 4  $\mu\text{m}$ , and report smaller particulate only above temperature of 850°C.

Calcination appears to significantly decrease the agglomeration of oxide particles.

## Feed

Feed material obtained from Russia was precipitated as Pu(IV) oxalate, and exhibits the typical square crystallites that are the expected morphology for Pu(IV) oxalate precipitates. [3] There are fewer aggregates in the feed fuel than in fuel examined after aqueous processing, consistent with the low surface energy and compact particle shapes in oxide produced via the Pu(IV) oxalate. Some agglomeration is expected, as observed here.

Surface energy is expected and known [5] to be low, but surface area in Pu(IV) oxalate particles may in fact be larger than anticipated. Medard and Madic report some coalescence of Pu(IV) particles below 800°C. [16] Observations made for  $^{239}\text{PuO}_2$  precipitated from Pu(IV) oxalate suggest that total surface area is larger than the exterior surface area for these compact crystals. Crowder et. al. report agglomerations of squares in Pu(IV) precipitates with specific surface areas 5 to 14  $\text{m}^2\text{g}^{-1}$ . [17] Smith reports specific surface areas of 5 to 10  $\text{m}^2\text{g}^{-1}$  in material calcined at 700°C where the particle dimensions would suggest a much lower surface area of 0.1 to 1  $\text{m}^2\text{g}^{-1}$ . These workers conclude that substantial surface area is contributed by interior surfaces.

Feed fuel examined here has been in storage for a number of years, but the expectation that particle size of this material may be decreased by the decay of the  $^{238}\text{PuO}_2$  and autoradiolytic fracture of particles is not borne out by observations presented here. Both particle size and shape are typical of  $\text{PuO}_2$  derived from unaged Pu(IV) oxalate. [3][6] Other measurements of  $^{238}\text{PuO}_2$  oxide suggest that autoradiolysis reduces particle size only for particles larger than about 10  $\mu\text{m}$ . [7][8] This observation is consistent with the path length of about 5  $\mu\text{m}$  for the helium produced during radiolysis, which allows helium to be expelled from small particles without producing gas bubbles or inclusions that impose strain on the structure. For comparison, high-fired granules of  $\text{PuO}_2$  fuel high-fired to 1200°C and sized to 70  $\mu\text{m}$  show an average particle size of 24  $\mu\text{m}$  after 2 months of aging. [9]

The observed particle sizes of 8  $\mu\text{m}$  and 12  $\mu\text{m}$  in lot SN-175 are consistent with particle fracture and size reduction due to autoradiolysis. However, the multimodal particle sizes between 30  $\mu\text{m}$  and 50  $\mu\text{m}$  in FSO-66 are not consistent with disintegration either of square laths or of agglomerated crystallites over time.

## Conclusions

Particle sizes observed in these few measurements are roughly consistent with previous reports, [1][2][3][6] and consistent with expectations for the conditions of precipitation,

and with nitric acid and oxalate concentrations. [1][2] Observed particle sizes are larger than would be consistent with the measured precipitation temperature, but the measured high degree of agglomeration is consistent with these temperatures. [1] The relatively high plutonium concentrations should also lead to a high degree of agglomeration and small particle sizes.

Single particle measurements which exclude agglomeration or superposition of particles suggest sizes consistent with previously reported fused rosettes. [3] Because of the propensity of  $\text{PuO}_2$  to agglomerate, the single particle images are useful in accurately describing precipitation behavior. Agglomerates are easily broken up during subsequent processing, and may not be relevant to granule formation or pellet pressing.

Particle sizes vary between aqueous processing runs. Single particle measurements vary less than measurements which include agglomerates, but even single particle measurements exhibit sufficient variation to confirm that differences exist between runs. The difference between particles measured in 2012 and those measured in 2018 and 2019 is particularly noticeable.

Calcination, as anticipated, [3] does not affect particle size. The temperature difference between spontaneous calcination and treatment in the  $650^\circ\text{C}$  calcination furnace temperature is not large.

The number of agglomerates is much higher than anticipated or than observed in previous examinations of oxide. [8][10] This may be an artifact of sample preparation which produces an image that is too dense in particles, or it may indicate real agglomeration in these samples.

For feed fuels, variations in measured particle sizes may indicate excessive superposition of particles during sample preparation, or may indicate variation is in agglomeration due to fuel feed processing. Little is known about preparation methods and process conditions for preparation of the feed fuel, except that fuel was prepared by  $\text{Pu(IV)}$  oxalate precipitation.

It is unfortunate that sampling was not performed on a larger number of distinct batches. Comparison of batches would allow better relation of particle size to process conditions. More comprehensive sampling of the various runs in future aqueous processing campaigns is anticipated.

## References

1. P. K. Smith, G. A. Burney, D. T. Rankin, D. F. Bickford, and R. D. Sisson, Jr., "Effect of Oxalate Precipitation on  $\text{PuO}_2$  microstructure," Savannah River Laboratory DP-MS-76-34 (1976.)
2. G.A. Burney and P.K. Smith, "Controlled  $\text{PuO}_2$  Particle Size from  $\text{Pu(III)}$  Oxalate Precipitation," Savannah River National Laboratory Report DP-1689 (1984.)
3. G.A. Burney and J.W. Congdon, "Direct Fabrication of  $^{238}\text{PuO}_2$  Fuel Forms," Savannah River National Laboratory Report DP-1621 (July 1982.)
4. B.A. Mueller, D.D. Rohr, and R.N.R. Mulford, Los Alamos National Laboratory Report LA-5524, Los Alamos National Laboratory (1974.)

5. J. Huling, Los Alamos National Laboratory, private communication.
6. R.M. Orr, H.E. Sims, and R.J. Taylor, *J. Nucl. Mats.*, **465**, pp. 756-773, (2015.)
7. J.G. Teague, M.A. Reimus, A.R. Herrera, and P.F. Moniz, "Fragmentation Response of Aged Milliwatt Fuel," Los Alamos National Laboratory Report LA-UR-02-3575 (2002).
8. R.N. Mulford, "Pu-238 Oxide Fuel Fracture Behavior as a Function of Age," Los Alamos National Laboratory, LA-UR-14-25228, proceedings of the INMM National Meeting, Atlanta, Ga. (2014.)
9. L. Brodnax, Los Alamos National Laboratory, private communication.
10. R.N. Mulford, B.L. Berger, and R. Chavarria "Particle Size in Ball-Milled  $^{238}\text{PuO}_2$  Oxide as a Function of Residence Time in Fuel Container," Los Alamos National Laboratory Report LA-CP-12-01240 (Sept 2012.)
11. W.S. Rasband, "Image J," U.S. National Institutes of Health, Bethesda, Maryland, USA, [imagej.nih.gov/ij/](http://imagej.nih.gov/ij/), 1997—2012.
12. R.N. Kelly, K.J. DiSante, E. Stranzl, J.A. Kazanjian, P. Bowen, T. Matsuyama, and N. Gabas, "Graphical Comparison of Image Analysis and Laser Diffraction Particle, Size Analysis Data Obtained From the Measurements of Nonspherical Particle Systems," *AAPS Pharm. Sci. Tech.* 2006; **7**(3) Article 69 (2006.)
13. R. Mulford and D. Spengler, "Bulk and rough tap densities of two granular fuel lots," Los Alamos National Laboratory Report LA-UR-16-24660, in proceedings of the INMM National Meeting, Atlanta Ga (2016.)
14. C.G.J. Baker and M.A. Bergougnou, *Can. J. Chem. Eng.*, **52**(2) pp. 246-250 (1974.)
15. D. Spengler, private communication.
16. X. Machuron-Mandard and C. Madic, "Plutonium dioxide particle properties as a function of calcination temperature," *J. of Alloys and Compounds*, **235**, pp. 216-224 (1996.)
17. M.L. Crowder and R.A. Pierce, "Lab Scale Demonstration of Plutonium Purification by Anion Exchange, Plutonium(IV) Oxalate Precipitation, and Calcination to Plutonium Oxide to Support the MOX Feed Mission," SNRL-STI-2012-00422, pp. 1-45 (2012.)